Pergamon

Int. J. Solids Structures Vol. 35, No. 7–8, pp. 719–731, 1998

0020–7683/98 $19.00 + .00

PII: S0020–7683(97)00071–1

TORSION OF TUBES OF ARBITRARY SHAPE

C. Y. WANG
Departments of Mathematics and Mechanical Engineering, Michigan State University, Wells Hall, East Lansing, MI 48824-1027, U.S.A.

(*Received* 8 *November* 1996; *in revised form* 21 *February* 1997)

Abstract—The method of eigenfunction expansion and matching can be applied to arbitrary shaped, hollow tubes which are described by curved and straight pieces. The method is highly efficient and superior to finite differences. The oval tube and the rounded polygonal tube are studied in detail. Approximate formula for torsional rigidity from membrane analogy is valid only for thin tubes with thickness less than 0.2. Maximum shear stress occurs either at re-entrant inner corners or at the outer boundary on the minor axis. © 1997 Elsevier Science Ltd

INTRODUCTION

The study of the torsion of bars is important and basic in the design of structural elements [Sokolnikoff (1956); Timoshenko and Goodier (1970)]. Analytic solutions have been found for some simple cross-sectional shapes such as the circle, annulus, ellipse, rectangle and triangle [Young (1989)]. Numerical integration is usually necessary for more complicated shapes.

For given mass, the hollow circular tube is most desirable, since it has the highest torsional rigidity per weight. However, due to restrictions in size, or due to ease of fastening, or due to aerodynamic considerations, hollow tubes are often made into oval, airfoil or polygonal shapes. Examples include struts, turbine blades, wrenches and beams. Recently, Wang (1995) studies the torsion of a flattened tube consisting of two half annular pieces and two rectangular pieces. That paper used an eigenfunction expansion and point match method which is more efficient than direct numerical integration. The present paper generalizes the method to treat arbitrary shapes. In addition, we shall use an integral form of collocation which is much smoother than the point-match collocation used previously. Specific results are obtained for a class of oval tubes and rounded regular polygonal tubes.

GENERAL CONSIDERATION

We assume the tube is of constant thickness (not necessarily thin) and the same cross-sectional shape. Its median boundary is a C' continuous closed curve, which can be approximated by M connected segments of circular arcs or straight lines [Fig. 1(a)]. The Prandtl stress function [Sokolnikoff (1956)] is governed by

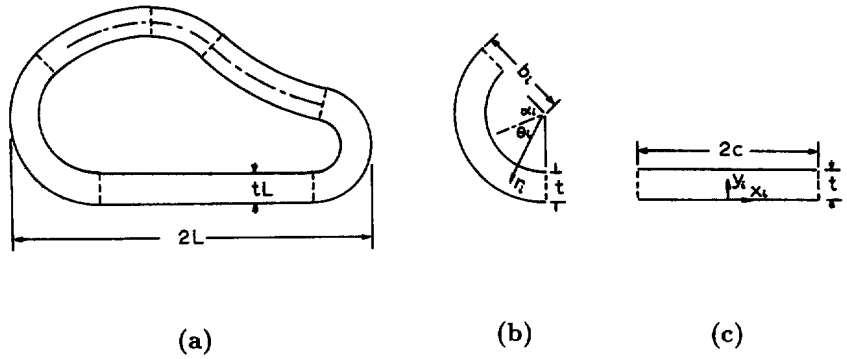

(a) (b) (c)

Fig. 1. (a) Cross-section of the hollow tube; (b) an annular piece; (c) a rectangular piece.

$$\nabla^2\psi = -2 \tag{1}$$

$$\psi = k \quad \text{on inner boundary}$$
$$\psi = 0 \quad \text{in outer boundary} \tag{2}$$

where the constant k is determined by

$$\oint_{\text{outer}} \frac{\partial\psi}{\partial\eta}\,\mathrm{d}\xi + 2A_{\text{outer}} = 0 \tag{3}$$

Here, all lengths have been normalized by some characteristic length L, ψ by L^2, η is the outward normal, ξ is the arc length and A_{outer} is the normalized area enclosed by the outer boundary. The idea is to solve each annular or rectangular piece satisfying eqns (1) and (2), match ψ and its derivative along adjacent boundaries, then use eqn (3) to determine k.

Suppose the ith piece is annular and convex, described by polar coordinates $a_i \leqslant r_i \leqslant b_i$, $-\alpha_i \leqslant \theta_i \leqslant \alpha_i$ [Fig. 1(b)]. The solution to eqns (1) and (2) is

$$\psi_i(r_i,\theta_i) = \frac{1}{2}(b_i^2 - r_i^2) - \left[\frac{1}{2}(b_i^2 - a_i^2) - k\right]\frac{\ln(r_i/b_i)}{\ln(a_i/b_i)} + \sum_{n=1}^{\infty} \sin\left[\lambda_{in}\ln(r_i/b_i)\right]\left[A_{in}\mathrm{e}^{\lambda_{in}(\theta_i-\alpha_i)} + B_{in}\mathrm{e}^{-\lambda_{in}(\theta_i+\alpha_i)}\right] \tag{4}$$

where $\lambda_{in} = n\pi/|\ln(a_i/b_i)| > 0$ is the eigenvalue and the factors $\exp(-\lambda_{in}\alpha_i)$ are to ensure the coefficients A_{in}, B_{in} remain reasonable magnitudes. If the ith piece is concave, eqn (4) can still be used except now $b_i < a_i$. If the ith piece is flat, described by cartesian coordinates $0 \leqslant y_i \leqslant t$, $-c_i \leqslant x_i \leqslant c_i$ [Fig. 1(c)]. The solution is in the form

$$\psi_i(x_i,y_i) = -y_i^2 + \left(t + \frac{k}{t}\right)y_i + \sum_{n=1}^{\infty} \sin(\kappa_n y_j)\left[A_{in}\mathrm{e}^{\kappa_n(x_j-c_j)} + B_{in}\mathrm{e}^{-\kappa_n(x_j+c_j)}\right] \tag{5}$$

where t = thickness $= |b_i - a_i|$ and $\kappa_n = n\pi/t$ is the eigenvalue.

The form of eqn (5) is a Fourier series whose convergence is well-known. The two sets of constants A_{in} and B_{in} can be adjusted to match any two given functions of y on the boundaries at $x_j = \pm c_j$. the convergence of eqn (4) can be demonstrated as follows. Let $s = \ln(r/b)/|\ln(a/b)|$ then the eigenfunction $\sin[\lambda_n \ln(r/b)]$ becomes $\sin(n\pi s)$ which is a complete Fourier series in $0 \leqslant |s| \leqslant 1$. Thus, any two given function of s (or r) can be represented at $\theta = \pm\alpha$. The convergence is absolute and uniform.

Now along each adjacent boundary of neighboring pieces the value of ψ and its normal derivative are to be matched, i.e.

$$\psi_i = \psi_{i+1}, \quad i = 1 \quad \text{to } M \quad (\psi_{M+1} = \psi_1) \tag{6}$$

$$\psi_i' = \psi_{k+1}', \quad i = 1 \quad \text{to } M \quad (\psi_{M+1}' = \psi_1') \tag{7}$$

where ψ_i' may be either $\partial\psi_i/\partial x_i$ or $1/r_i\,\partial\psi_i/\partial\theta_i$. There are $2M$ sets of conditions for the $2M$ sets of unknowns A_{in}, B_{in}. Equation (3) then gives k

$$\sum_{i=1}^{M} P_i + 2A_{\text{outer}} = 0 \tag{8}$$

where P_i is either $\int_{-\alpha_i}^{\alpha_i} r_i\,\partial\psi_i/\partial r_i|_{b_i}\,\mathrm{d}\theta_i$ or $\int_{-c_i}^{c_i} -\partial\psi_i/\partial y_i|_0\,\mathrm{d}x_i$.

Each infinite series is truncated to N terms, where the linear eqns (6)–(8) represent $2MN+1$ equations and $2MN+1$ unknowns. Convergence is usually very fast. Since ψ is complete and both ψ and ψ' are matched on the boundary, the series representations for each piece would converge to the unique exact solution as $N \to \infty$.

The torsional rigidity, normalized by 2 (Lamé constant) L^4 is then

$$D = \int\int \psi \, d\sigma + kA_{\text{inner}} \tag{9}$$

where σ is the area of the tube wall. The details are illustrated in the following examples.

THE OVAL TUBE

Figure 2(a) shows a symmetric oval tube of constant thickness which is composed of four symmetrically placed annular sector pieces. Let the length scale be half the chord length (normalized chord length = 2), given the aspect ratio R, the minimum outer radius b_1 and thickness t we find from geometry

$$b_2 = \frac{1-2b_1+1/R}{2(1/R-b_1)} \tag{10}$$

$$\alpha_2 = \sin^{-1}\left(\frac{1-b_1}{b_2-b_1}\right), \quad \alpha_1 = \frac{\pi}{2}-\alpha_2 \tag{11}$$

$$a_1 = b_1 - t, \quad a_2 = b_2 - t \tag{12}$$

$$A_{\text{inner}} = 2(a_1^2\alpha_1 + a_2^2\alpha_2) - (a_2-a_1)^2 \sin(2\alpha_2) \tag{13}$$

$$A_{\text{outer}} = 2(b_1^2\alpha_1 + b_2^2\alpha_2) - (b_2-b_1)^2 \sin(2\alpha_2). \tag{14}$$

Due to symmetry the solution to each piece is given as

$$\psi_1(r_1,\theta_1) = \frac{1}{2}(b_1^2-r_1^2) - \left[\frac{1}{2}(b_1^2-a_1^2) - k\right]\frac{\ln(r_1/b_1)}{\ln(a_1/b_1)} + \sum_{n=1}^{N} A_{1n}\varphi_{1n}(r_1)[e^{\lambda_{1n}(\theta_1-\alpha_1)} + e^{-\lambda_{1n}(\theta_1+\alpha_1)}] \tag{15}$$

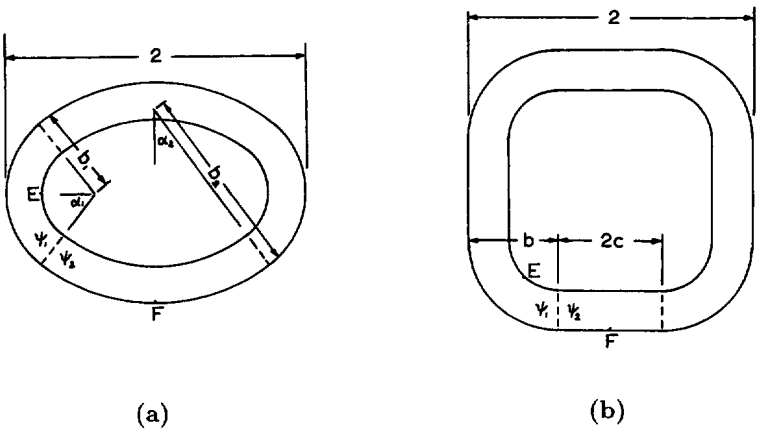

(a) (b)

Fig. 2. (a) The oval tube; (b) the rounded polygonal tube.

$$\psi_2(r_2,\theta_2)=\frac{1}{2}(b_2^2-r_2^2)-\left[\frac{1}{2}(b_2^2-a_2^2)-k\right]\frac{\ln(r_2/b_2)}{\ln(a_2/b_2)}$$
$$+\sum_{n=1}^{N}A_{2n}\varphi_{2n}(r_2)[e^{\lambda_{2n}(\theta_2-\alpha_2)}+e^{-\lambda_{2n}(\theta_2+\alpha_2)}] \quad (16)$$

where

$$\varphi_{1n}(r_1)=\sin[\lambda_{1n}\ln(r_1/b_1)],\quad \varphi_{2n}(r_2)=\sin[\lambda_{2n}\ln(r_2/b_2)] \quad (17)$$

and

$$\lambda_{1n}=\frac{-n\pi}{\ln(a_1/b_1)},\quad \lambda_{2n}=\frac{-n\pi}{\ln(a_2/b_2)}. \quad (18)$$

The matching conditions are

$$\psi_1(r_1,\alpha_1)=\psi_2(r_2,-\alpha_2)|_{r_2\to b_2-b_1+r_1} \quad (19)$$

$$\frac{1}{r_1}\frac{\partial\psi_1}{\partial\theta_1}(r_1,\alpha_1)=\frac{1}{r_2}\frac{\partial\psi_2}{\partial\theta_2}(r_2,-\alpha_2)|_{r_2\to b_2-b_1+r_1}. \quad (20)$$

The following properties of the eigenfunction φ_{1n} can be derived:

$$\int_{a_1}^{b_1}\frac{1}{r_1}\varphi_{1m}(r_1)\varphi_{1n}(r_1)\,dr_1=\begin{cases}0 & m\neq n\\ \frac{1}{2}\ln\left(\frac{b_1}{a_1}\right) & m=n\end{cases} \quad (21)$$

$$\int_{a_1}^{b_1}r_1^{\nu-1}\varphi_{1n}(r_1)\,dr_1=-\frac{\lambda_{1n}}{\nu^2+\lambda_{1n}^2}[b_1^{\nu}-a_1^{\nu}(-1)^n] \quad (22)$$

$$\int_{a_1}^{b_1}\frac{1}{r_1}\ln\left(\frac{r_1}{b_1}\right)\varphi_{1n}(r_1)\,dr_1=\frac{(-1)^n}{\lambda_{1n}}\ln\left(\frac{a_1}{b_1}\right). \quad (23)$$

Instead of using point-match, eqn (19) is multiplied by $\varphi_{1m}(r_1)/r_1$ and integrated from a_1 to b_1. After some work, the result is

$$k\left[\frac{I_m}{\ln(a_2/b_2)}-\frac{(-1)^m}{\lambda_{1m}}\right]-A_{1m}\frac{1}{2}\ln\left(\frac{b_1}{a_1}\right)(1+e^{-2\lambda_{1m}\alpha_1})+\sum_{n=1}^{N}A_{2n}J_{mn}(1+e^{-2\lambda_{2n}\alpha_2})$$
$$=b_1(b_2-b_1)\frac{(1-(-1)^m)}{\lambda_{1m}}-(b_2-b_1)\frac{\lambda_{1m}}{1+\lambda_{1m}^2}[b_1-a_1(-1)^n]$$
$$-\frac{(b_1^2-a_1^2)(-1)^m}{2\lambda_{1m}}+\frac{(b_2^2-a_2^2)I_m}{2\ln(a_2/b_2)},\quad m=1\ \text{ to } N \quad (24)$$

where

$$I_m \equiv \int_{a_1}^{b_1} \frac{1}{r_1} \ln\left(\frac{b_2 - b_1 + r_1}{b_2}\right) \varphi_{1m}(r_1)\, dr_1 \tag{25}$$

$$J_{mn} \equiv \int_{a_1}^{b_1} \frac{1}{r_1} \varphi_{1m}(r_1)\varphi_{2n}(b_2 - b_1 + r_1)\, dr_1 \tag{26}$$

are numerically evaluated. Similarly, eqn (20) gives

$$A_{1m}\frac{1}{2}\ln\left(\frac{b_1}{a_1}\right)\lambda_{1m}(1-e^{-2\lambda_{1m}\alpha_1}) + \sum_{n=1}^{N} A_{2m}H_{mn}\lambda_{2n}(1-e^{-2\lambda_{2n}\alpha_2}) = 0, \quad m = 1 \quad \text{to } N \tag{27}$$

where

$$H_{mn} \equiv \int_{a_1}^{b_1} \frac{1}{b_2 - b_1 + r_1} \varphi_{1m}(r_1)\varphi_{2n}(b_2 - b_1 + r_1)\, dr_1. \tag{28}$$

The condition eqn (3) is

$$4\left[\int_0^{\alpha_1} \left(\frac{\partial \psi_1}{\partial r_1} r_1\right)_{b_1} d\theta_1 + \int_{-\alpha_2}^{0} \left(\frac{\partial \psi_2}{\partial r_2} r_2\right)_{b_2} d\theta_2\right] + 2A_{\text{outer}} = 0. \tag{29}$$

This yields

$$k\left[\frac{\alpha_1}{\ln(a_1/b_1)} + \frac{\alpha_2}{\ln(a_2/b_2)}\right] + \sum_{n=1}^{N} A_{1n}(1-e^{-2\lambda_{1n}\alpha_1}) + \sum_{n=1}^{N} A_{2n}(1-e^{-2\lambda_{2n}\alpha_2})$$
$$= \frac{(b_1^2 - a_1^2)\alpha_1}{2\ln(a_1/b_1)} + \frac{(b_2^2 - a_2^2)\alpha_2}{2\ln(a_2/b_2)} + \frac{1}{2}(b_2 - b_1)^2 \sin(2\alpha_2). \tag{30}$$

Equations (24), (27) and (30) are linear algebraic equations easily inverted for the $2N+1$ unknowns, A_{1n}, A_{2n}, k. The accuracy is refined by increasing N. The convergence is very fast. From eqn (9) the torsional rigidity is

$$D = \frac{\alpha_1}{2}(b_1^2 - a_1^2)^2 + \frac{(b_1^2 - a_1^2 - 2k)\alpha_1}{2\ln(a_1/b_1)}\left[b_1^2 + a_1^2\left(2\ln\left(\frac{a_1}{b_1}\right) - 1\right)\right]$$
$$- 4\sum_{n=1}^{N} A_{1n}\frac{[b_1^2 - a_1^2(-1)^n]}{4 + \lambda_{1n}^2}(1 - e^{-2\lambda_{1n}\alpha_1})$$
$$+ \frac{\alpha_2}{2}(b_2^2 - a_2^2)^2 + \frac{(b_2^2 - a_2^2 - 2k)\alpha_2}{2\ln(a_2/b_2)}\left[b_2^2 + a_2^2\left(2\ln\left(\frac{a_2}{b_2}\right) - 1\right)\right]$$
$$- 4\sum_{n=1}^{N} A_{2n}\frac{[b_2^2 - a_2^2(-1)^n]}{4 + \lambda_{2n}^2}(1 - e^{-2\lambda_{2n}\alpha_2})$$
$$+ 2k[a_1^2\alpha_1 + a_2^2\alpha_2 - (a_2 - a_1)^2 \cos\alpha_2 \sin\alpha_2]. \tag{31}$$

Table 1.

	$t = 0.4$	$t = 0.1$
$N = 1$	0.4237	0.1785
3	0.4223	0.1785
5	0.4221	0.1785
7	0.4221	—

As an illustration of how fast the convergence is, Table 1 shows some typical results for rigidity D as N is increased. (aspect ratio = 1.25, $b_1 = 0.5$).

We see the convergence is slightly slower for thicker tubes. Unless t is very close to b_1, inducing a sharp corner, the one-term ($N = 1$) result is within 1% of the asymptote as $N \to \infty$. Thus, solving eqns (24), (27) and (30) using $N = 1$ is usually sufficient. The three equations and three unknowns can be inverted almost analytically. If t is close to b_1, convergence is much slower and one may improve the rate of convergence of the Fourier series by the methods of Kantorovich and Krylov (1958).

The maximum shear stress (normalized by (Lamé constant) · L) occurs either at point E or point F in Fig. 2(a)

$$\tau_m = \frac{\partial \psi_1}{\partial r_1}(a_1, 0) = -a_1 - \frac{(b_1^2 - a_1^2 - 2k)}{2a_1 \ln(a_1/b_1)} + 2\sum_{n=1}^{N} A_{1n}(-1)^n \frac{\lambda_{1n}}{a_1} e^{-\lambda_{1n}\alpha_1} \tag{32}$$

$$\tau_m = \frac{\partial \psi_2}{\partial r_2}(b_2, 0) = -b_2 - \frac{(b_2^2 - a_2^2 - 2k)}{2b_2 \ln(a_2/b_2)} + 2\sum_{n=1}^{N} A_{2n} \frac{\lambda_{2n}}{b_2} e^{-\lambda_{2n}\alpha_2}. \tag{33}$$

THE ROUNDED REGULAR POLYGONAL TUBE

The cross-section of the tube is composed of annular sectors and rectangles [Fig. 2(b)]. Let K be the number of sides and $2L$ be the minimum width. From geometry one can show $\alpha = \pi/K$,

$$A_{\text{inner}} = \pi a^2 + 2acK + c^2 \cot(\alpha) K \tag{34}$$

$$A_{\text{outer}} = \pi b^2 + 2bcK + c^2 \cot(\alpha) K \tag{35}$$

and c is related to b from Table 2.

Table 2.

K	c
3	$2(1-b)/\sqrt{3}$
4	$(1-b)$
5	$[(1-b)]/[\cos(3\pi/10) + \cos(\pi/10)]$
6	$(1-b)/\sqrt{3}$
8	$(1-b)/(1+\sqrt{2})$
12	$(1-b)/(2+2/\sqrt{3})$

Due to symmetry, we need to consider only two pieces

$$\psi_1(r,\theta) = \frac{1}{2}(b^2-r^2) - \left[\frac{1}{2}(b^2-a^2) - k\right]\frac{\ln(r/b)}{\ln(a/b)} + \sum_{n=1}^{N} A_n \varphi_n(r)(e^{\lambda_n(\theta-\alpha)} + e^{-\lambda_n(\theta+\alpha)}) \quad (36)$$

$$\psi_2(x,y) = -y^2 + \left(t + \frac{k}{t}\right)y + \sum_{n=1}^{N} B_n \sin(\kappa_n y)(e^{\kappa_n(x-c)} + e^{-\kappa_n(x+c)}) \quad (37)$$

where $\lambda_n = -n\pi/\ln(a/b)$ and $\kappa_n = n\pi/t$. The matching conditions are

$$\psi_1(r,\alpha) = \psi_2(-c, b-r) \quad (38)$$

$$\frac{1}{r}\frac{\partial \psi_1}{\partial \theta}(r,\alpha) = \frac{\partial \psi_2}{\partial x}(-c, b-r). \quad (39)$$

Again these are integrated with the weights φ_m/r and φ_m, respectively, to yield

$$\begin{aligned} &k\left[\frac{(-1)^m}{\lambda_m} + \frac{b}{t\lambda_m}(1-(-1)^m) - \frac{\lambda_m}{t(1+\lambda_m^2)}(b-a(-1)^m)\right] \\ &\quad + A_m \frac{1}{2}\ln\left(\frac{b}{a}\right)(1+e^{-2\lambda_m\alpha}) - \sum_{n=1}^{N} B_n S_{mn}(1+e^{-2\kappa_n c}) \\ &= \left(\frac{3}{2}b^2 - tb\right)\frac{1}{\lambda_m}(1-(-1)^m) + (t-2b)\frac{\lambda_m}{1+\lambda_m^2}(b-a(-1)^m) \\ &\quad + \frac{\lambda_m}{2(4+\lambda_m^2)}(b^2-a^2(-1)^m) + \frac{1}{2}(b^2-a^2)\frac{(-1)^m}{\lambda_m}, \quad m = 1 \text{ to } N \end{aligned} \quad (40)$$

$$A_m \frac{1}{2}\ln\left(\frac{b}{a}\right)\lambda_m(1-e^{-2\lambda_m\alpha}) + \sum_{n=1}^{N} B_n T_{mn}\kappa_n(1-e^{-2\kappa_n c}), \quad m = 1 \text{ to } N \quad (41)$$

where

$$S_{mn} \equiv \int_a^b \frac{1}{r}\sin(\kappa_n(b-r))\varphi_m(r)\,dr \quad (42)$$

$$T_{mn} \equiv \int_a^b \sin(\kappa_n(b-r))\varphi_m(r)\,dr \quad (43)$$

are to be evaluated by quadrature. Equation (3) becomes

$$\begin{aligned} &k\left[\frac{\alpha}{\ln(a/b)} - \frac{c}{t}\right] + \sum_{n=1}^{N} A_n(1-e^{-2\lambda_n\alpha}) + \sum_{n=1}^{N} B_n(e^{-2\kappa_n c} - 1) \\ &\qquad = b^2\alpha + \frac{(b^2-a^2)\alpha}{2\ln(a/b)} - \frac{\pi b^2}{K} + ct - 2cb - c^2\cot(\alpha). \end{aligned} \quad (44)$$

Equations (40), (41) and (44) are to be solved for A_n, B_n and k. The convergence is again very fast. The torsional rigidity is

$$D = 2K\left\{\frac{\alpha}{8}(b^2-a^2)^2 + \frac{(b^2-a^2-2k)\alpha}{8\ln(a/b)}\left[b^2+a^2\left(2\ln\left(\frac{a}{b}\right)-1\right)\right]\right.$$
$$-\sum_{n=1}^{N} A_n \frac{(b^2-a^2(-1)^n)}{4\lambda_n^2}(1-e^{-2\lambda_n\alpha}) + \left(\frac{t^3}{6}+\frac{kt}{2}\right)c$$
$$\left.+\sum_{n=1}^{N} B_n \frac{1}{\kappa_n^2}(1-(-1)^n)(1-e^{-2\kappa_n c})\right\}$$
$$+k[\pi a^2 + 2acK + c^2\cot(\alpha)K]. \tag{45}$$

The maximum shear is either at point E or point F:

$$\tau_m = \frac{\partial\psi_1}{\partial r}(a,0) = -a - \frac{(b^2-a^2-2k)}{2a\ln(a/b)} + 2\sum_{n=1}^{N} A_n(-1)^n \frac{\lambda_n}{a} e^{-\lambda_n\alpha} \tag{46}$$

$$\tau_m = \frac{\partial\psi_2}{\partial y}(0,0) = t + \frac{k}{t} + 2\sum_{n=1}^{N} B_n\kappa_n e^{-\kappa_n c}. \tag{47}$$

RESULTS AND DISCUSSION

For the oval tube the parameters are aspect ratio R, minimum outer radius b_1 and thickness t. Their ranges are restricted by $0 < t < b_1 < 1/R$. Figure 3(a) shows the torsional rigidity as a function of the ratio t/b_1 for various constant b_1 (aspect ratio $R = 1.25$). The $b_1 = 1/R = 0.8$ limit was computed by letting $b_1 = 0.799$. The result agrees with that from Wang (1995) for a tube consisting of two annular pieces and two straight pieces. Also shown in the figure is the empirical formula from membrane analogy [Timoshenko and Goodier (1970)]

$$D \approx \frac{2(\text{mean area})^2 t}{\text{mean perimeter}} = \frac{(A_{\text{outer}} + A_{\text{inner}})^2 t}{4(\alpha_1 b_1 + \alpha_2 b_2 + \alpha_1 a_1 + \alpha_2 a_2)}. \tag{48}$$

Equation (48) is surprisingly accurate for small t ($t < 0.2$). The corresponding maximum shear stress is shown in Fig. 3(b). For high values of b_1 the maximum occurs at point F in Fig. 2(a), but switches to point E for smaller b_1 or larger t.

Point E is an inner re-entrant corner where the stress becomes infinite as the corner becomes sharp ($t/b_1 \to 1$). Figure 3(b) shows the shear stresses at both places should be considered in the design of hollow torsion elements. For the prediction of maximum shear stress, the membrane analogy is too inaccurate to be compared. The results for larger aspect ratios are depicted in Figs 4 and 5.

Tubes whose cross-sections are described by confocal ellipses look similar to the ovals considered in this paper. However, the elliptic tubes do not have constant wall thickness. Not only are they more difficult to manufacture, the torsion properties are also undesirable, since the thinnest region of the tube is along the minor axis where the stresses are already high.

Figure 6(a) shows the torsional rigidity for the rounded square tube ($K = 4$). For clarity we plotted D vs t for various constant b. When $b = 1$ we recover the exact solution for a hollow circular tube

$$D = \frac{\pi}{4}[1-(1-t)^4]. \tag{49}$$

Also shown is the approximate formula for small t equivalent to eqn (48)

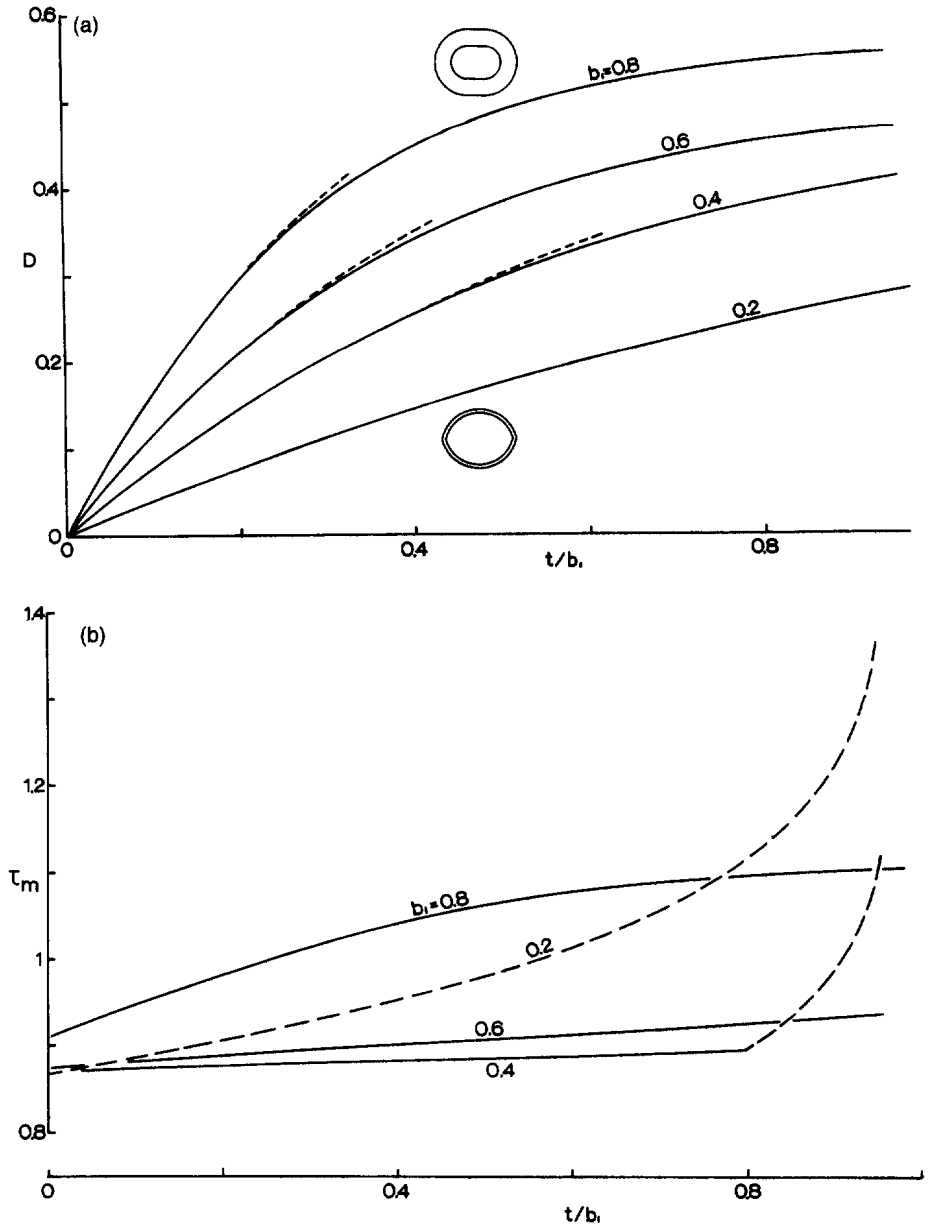

Fig. 3. Oval tube aspect ratio = 1.25: (a) torsional rigidity. Dashed lines are from eqn (48); (b) maximum shear stress. Solid lines: eqn (33) at point F, dashed lines: eqn (32) at point E.

$$D \approx \frac{[\pi(b^2+a^2)+2c(b+a)K+2c^2K\cot(\alpha)]^2 t}{2[\pi(a+b)+2cK]}. \tag{50}$$

The corresponding maximum shear stress is shown in Fig. 6(b). Depending on the thickness and rounding, the maximum shear stress may occur at either point E or point F. The results for the rounded hexagonal tube ($K = 6$) are shown in Fig. 7. For even larger K the results tend to the hollow circular tube, except at possible re-entrant corners where the shear stress may be high.

CONCLUSIONS

In this paper we introduced a method to solve the torsion problem of any smooth, constant-thickness hollow tube [Fig. 1(a)]. The method is accurate and highly efficient. In

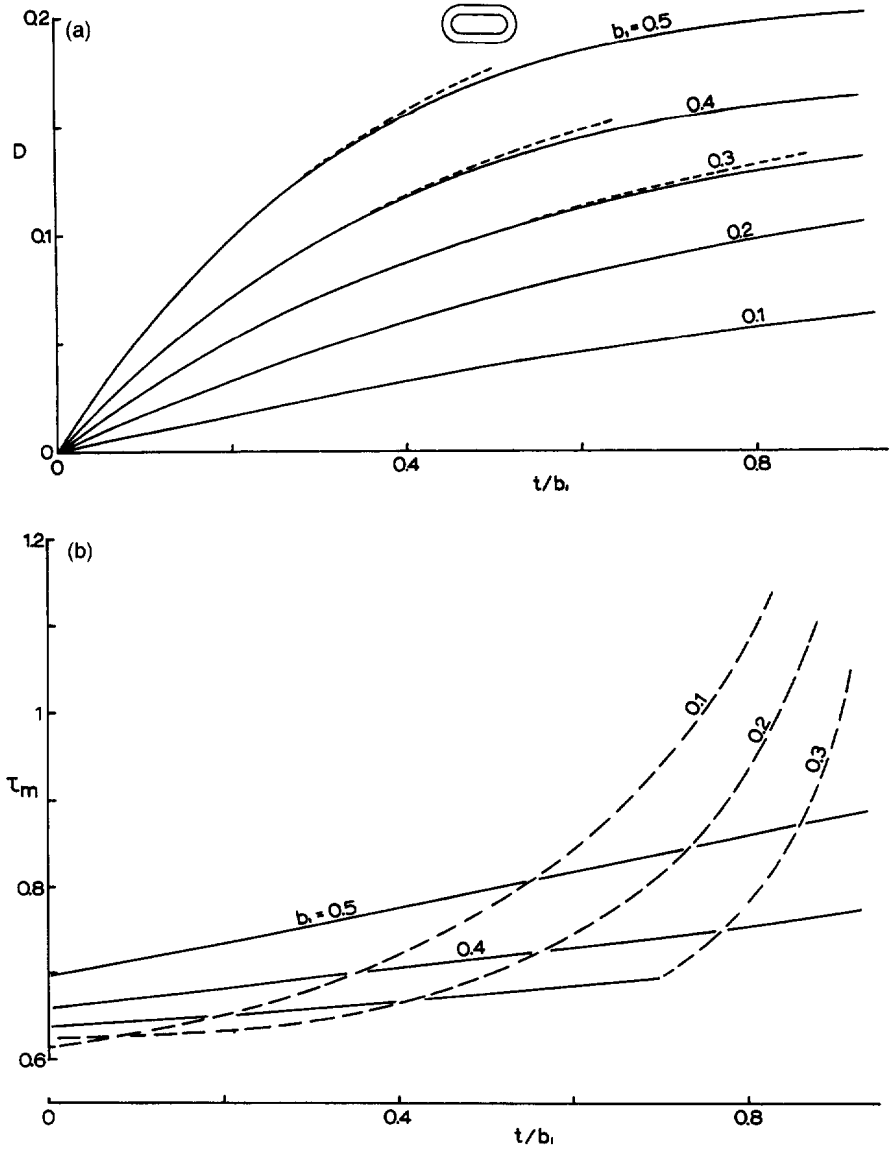

Fig. 4. Same legend as Fig. 3, except aspect ratio = 2.

comparison, the method of finite differences not only has to contend with curved boundaries, the required number of computations is more than the square of that used in this paper.

In matching the eigenfunction solutions for adjacent pieces, one can use point match [Wang (1995)] or other methods for collocation [Kolodziej (1987)]. Due to the skewness of the eigenfunction, the placement of collocation points has been a problem. We find integration weighted with the smaller radii eigenfunction voids this uncertainty. In addition, due to orthogonality, the coefficients of the more skewed eigenfunction are isolated.

It has long been recognized hollow tubes should have rounded corners. The re-entrant inner corner has little effect on torsional rigidity, but causes a high local shear stress. Our investigation shows, depending on geometry, the maximum shear stress may or may not occur at the re-entrant inner corner. In certain cases it occurs at the outside surface on the minor axis. Membrane analogies could not accurately estimate this maximum shear stress, even for thin tubes. Lastly, we obtain results for some classes of hollow tubes in the shape of ovals and rounded polygons. Our Figs 3–7 should be highly useful in the design of hollow torsion elements.

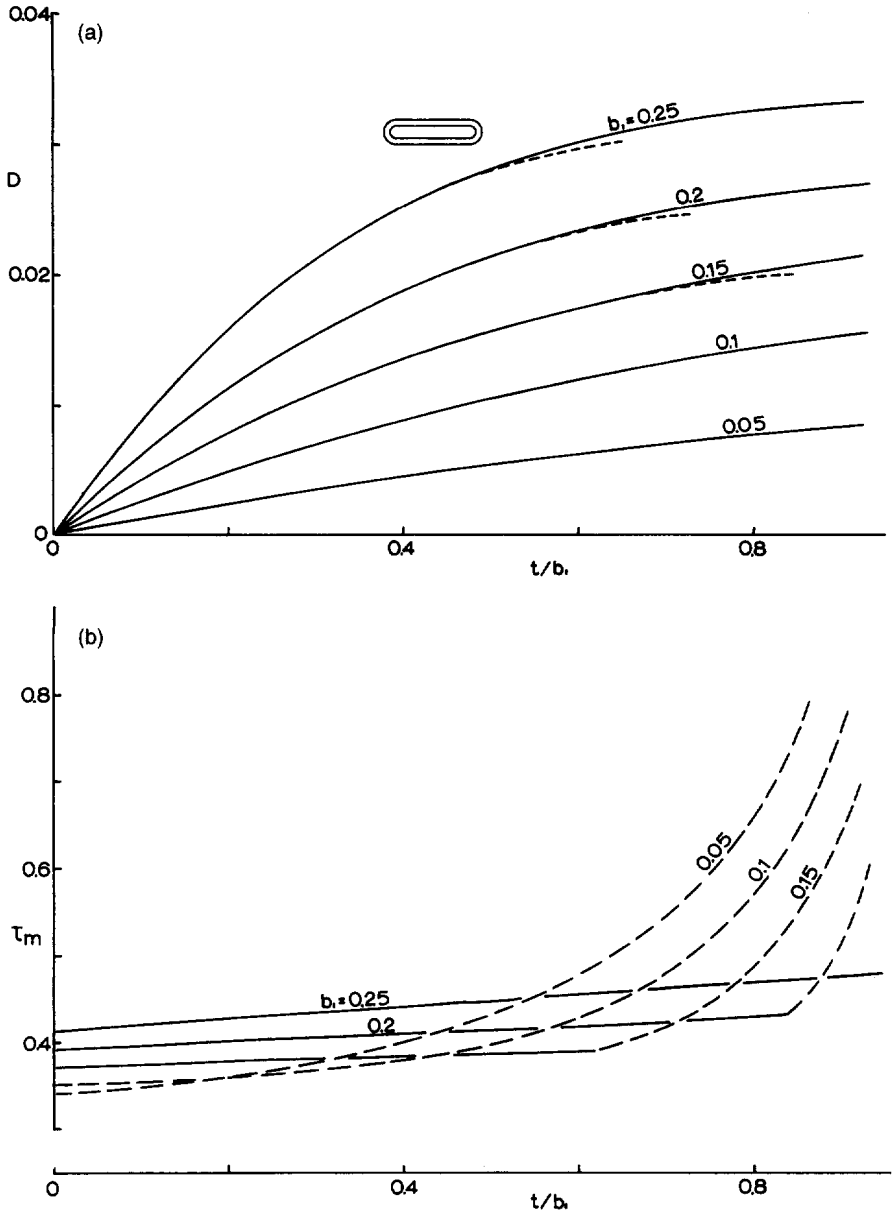

Fig. 5. Same legend as Fig. 3, except aspect ratio = 4.

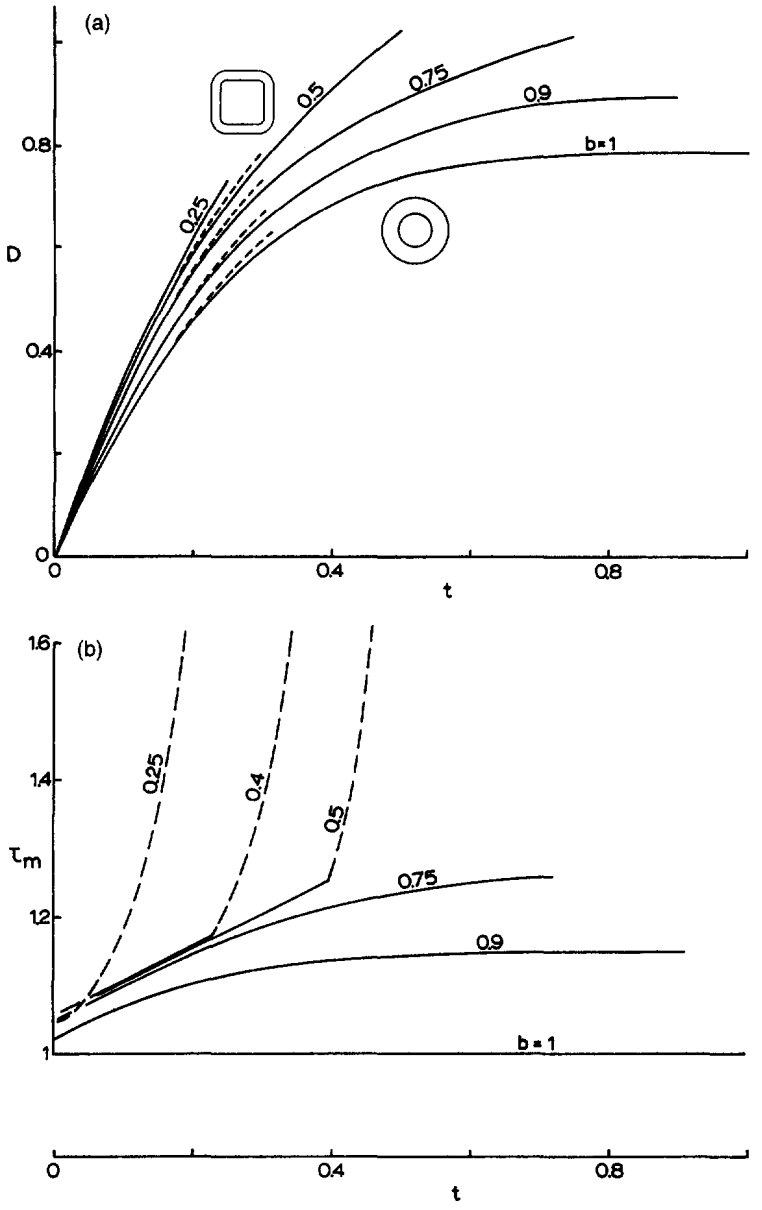

Fig. 6. Rounded square tube ($K = 4$): (a) torsional rigidity. Dashed lines are from eqn (50); (b) maximum shear stress. Solid lines: eqn (47) at point F, dashed lines: eqn (46) at point E.

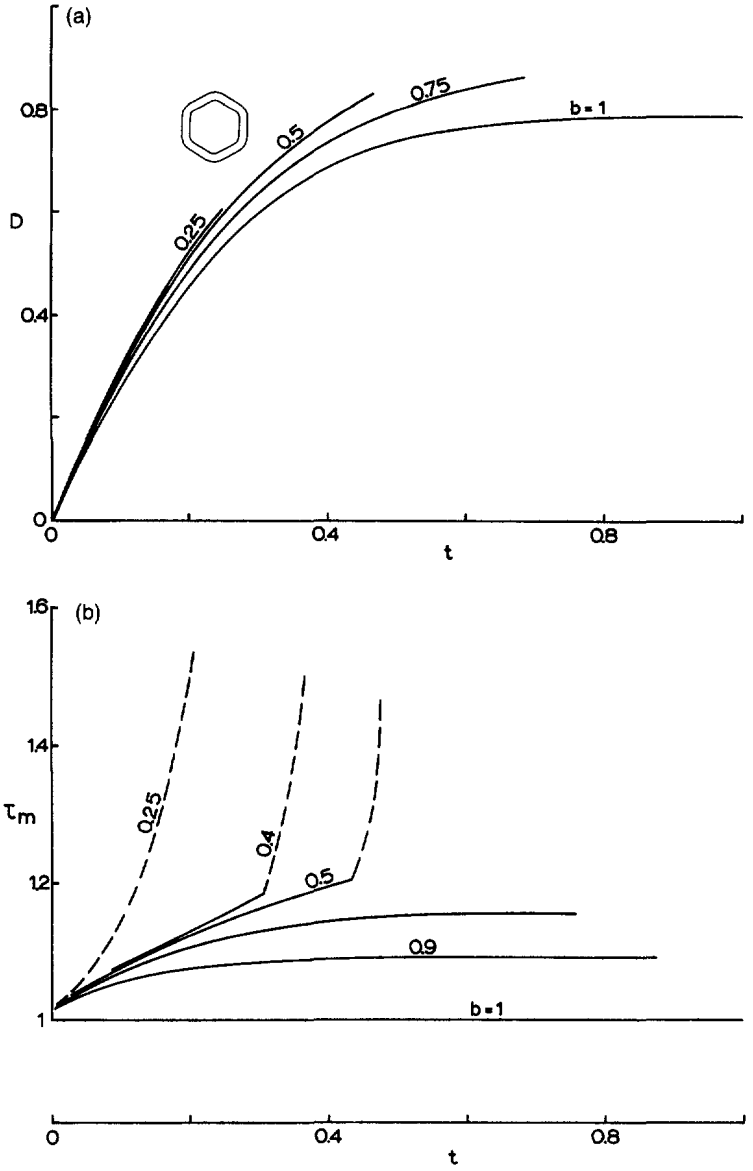

Fig. 7. Rounded hexagonal tube ($K = 6$): (a) torsional rigidity; (b) maximum shear stress.

REFERENCES

Kantorovich, L. V. and Krylov, V. I. (1958) *Approximate Methods of Higher Analysis*. Interscience, New York.
Kolodziej, J. A. (1987) Review of application of boundary collocation methods in mechanics of continuous media. *Solid Mechanics Archives*, **12**, 187–231.
Sokolnikoff, I. S. (1956) *Mathematical Theory of Elasticity*, 2nd edn. McGraw-Hill, New York.
Timoshenko, S. P. and Goodier, J. N. (1970) *Theory of Elasticity*, 3rd edn. McGraw-Hill, New York.
Wang, C. Y. (1995) Torsion of a flattened tube. *Meccanica*, **30**, 221–227.
Young, W. C. (1989) *Roark's Formulas for Stress and Strain*, 6th edn. McGraw-Hill, New York.